

Sliding wear: role of plasticity

R. Xu^{1,2,3} and B.N.J. Persson^{1,2,3}

¹*Peter Grünberg Institute (PGI-1), Forschungszentrum Jülich, 52425, Jülich, Germany*

²*State Key Laboratory of Solid Lubrication, Lanzhou Institute of Chemical Physics, Chinese Academy of Sciences, 730000 Lanzhou, China*

³*MultiscaleConsulting, Wolfshovener str. 2, 52428 Jülich, Germany*

Abstract: We present experimental wear data for polymethyl methacrylate (PMMA) sliding on tile, sandpaper, and polished steel surfaces, as well as for soda-lime, borosilicate, and quartz glass sliding on sandpaper. The experimental results are compared with a recently developed theory of sliding wear[1]. Our findings demonstrate that wear on surfaces with roughness below a critical threshold cannot result from crack propagation induced by frictional shear stress in block-substrate asperity contact regions and must, therefore, originate from a different mechanism.

Corresponding author: B.N.J. Persson, email: b.persson@fz-juelich.de

1 Introduction

Wear is the progressive loss of material from a solid body due to its contact and relative movement against a surface [2–11]. Wear particles can have an adverse influence on the health of living organisms, or result in the breakdown of mechanical devices. There are several limiting wear processes, known as *fatigue wear*, *abrasive wear*, and *adhesive wear*.

Fatigue wear occurs when a polymer block slides on a rigid countersurface with “smooth roughness.” In this scenario, the stress concentrations in asperity contact regions are relatively low, requiring multiple contacts to remove polymer particles. This wear process involves fatigue failure rather than tensile failure, where material removal is gradual. The abrasion caused by this failure mode is known as fatigue wear.

Abrasive wear, in contrast, arises when a polymer block slides against surfaces with sharp asperities. High stress concentrations at the asperity tips cut into the polymer, potentially exceeding the material’s limiting strength, leading to micro-cutting or scratching. This results in longitudinal scratches, called score lines, parallel to the sliding direction. Abrasive wear is primarily driven by mechanical interactions between the harder surface asperities and the softer polymer, making it distinct from fatigue wear.

Adhesive wear involves the transfer of material between contacting surfaces due to adhesive forces. It frequently occurs when one block slides on another block made of the same material. For example, in metallic systems, “cold-welded” junctions can form in the contact regions, and as these junctions break during sliding, the material is transferred from one surface to the other.

Many polymers have important medical applications,

but sometimes polymer wear results in severe health or other problems. For example, high-density polyethylene (HDPE) or ultra-high-molecular-weight polyethylene (UHMWPE) has been used as a bearing component in total joint replacements. However, the wear of HDPE and UHMWPE when sliding on the counter surface generates small polymer particles, which can induce an inflammatory response in the surrounding tissue, leading to osteolysis, where bone tissue is resorbed [12]. Over time, this may result in implant loosening or failure. Similarly, polymethyl methacrylate (PMMA) is commonly used for prosthetic dental applications, including the fabrication of artificial teeth, where wear may limit the useful lifetime.

Understanding crack propagation is essential for analyzing polymer wear. The crack or tearing energy γ (defined as the energy per unit area required to separate surfaces at a crack tip) provides a key measure of material resistance to crack growth [13]. For polymers, γ can range from $\sim 10^2$ to $\sim 10^5$ J/m², depending on factors such as crack tip velocity and temperature. This should be compared to the crack energy for (brittle) crystalline solids, which is on the order of ~ 1 J/m², even for solids with strong covalent bonds like diamonds. The large γ values in polymers arise from energy contributions due to chain stretching, uncrosslinked chain pull-out, and mechanisms like crazing, cavitation, and viscoelastic dissipation near the crack tip.

The crack energy γ has been extensively studied in cases of constant crack tip velocity [14] and oscillating strains [15–17], both yield similar results. Under oscillatory strain, the crack tip displacement Δx per strain cycle depends on γ . Below a lower critical value γ_0 (e.g., ~ 50 J/m² for PMMA), no crack growth occurs, while Δx diverges as γ approaches the ultimate tear strength γ_1 (e.g., ~ 500 J/m² for PMMA). However, unless γ is close to γ_1 , the crack tip displacement Δx is very small. Hence, several stress cycles may be needed to remove a particle from a PMMA surface under *fatigue wear*.

Crack energy is commonly characterized using macroscopic samples with characteristic dimensions on the order of ~ 1 cm. However, this macroscopic scale may not accurately capture the fracture behavior relevant to polymer wear, where material loss involves particles as small as ~ 1 μm . At such small scales, the influence of mechanisms like cavitation and crazing may be reduced. Moreover, the deformation in sliding contacts involves a wide distribution of frequencies, approximately given by $\omega \approx v/r_0$ (with v as the sliding speed and r_0 as the characteristic contact radius), in contrast to the single-frequency conditions typically applied in standard tearing energy tests.

In Ref. [1], a theory was developed to describe sliding wear in rubber. In this study, we extend this theory to PMMA and glass. Wear rates of PMMA sliding on tile, sandpaper, and polished steel surfaces under dry conditions, as well as glass sliding on sandpaper, are measured and compared with theoretical predictions.

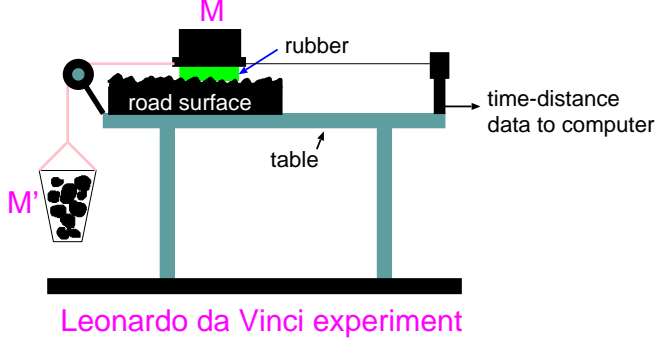


FIG. 1. A simple friction slider (schematic) measures the sliding distance $x(t)$ via a displacement sensor.

2 Experimental methods

The data used in the present study were obtained using the setup shown in Fig. 1. The slider consists of a block (PMMA or glass) glued to a metal plate. The nominal contact area is $A_0 \approx 20$ cm^2 . The normal force F_N is determined by the total mass M of lead blocks placed on top of the metal plate. Similarly, the driving force is controlled by the total mass M' of lead blocks placed in the container. The PMMA block was tested on three different substrates: ceramic tile, sandpaper P100, and polished steel. Three types of glass: soda-lime (window glass), borosilicate, and quartz glass, were tested on sandpaper P100.

The sliding distance $x(t)$ as a function of time t is measured using a displacement sensor. This simple friction slider setup can also be used to calculate the friction coefficient $\mu = M'/M$ as a function of sliding velocity and nominal contact pressure $p_0 = Mg/A_0$. Note that with this setup, the driving force is specified, allowing the

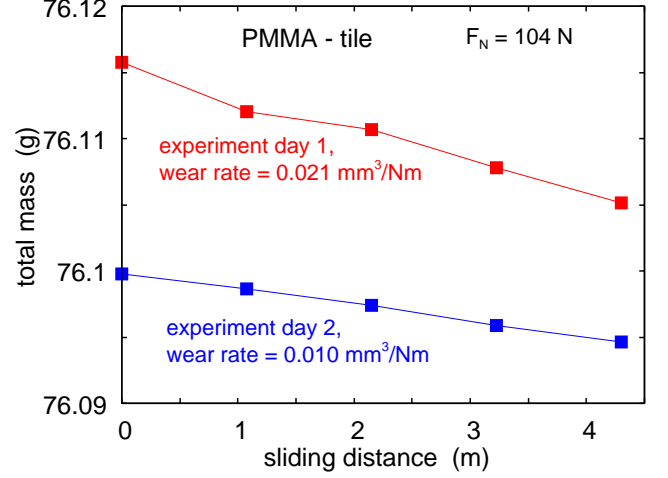


FIG. 2. The mass of the PMMA blocks and metal plate as a function of the sliding distance on the tile surface. Experiments performed on two consecutive days gave different wear rates $\Delta V/F_N L$ indicated in the figure.

study of the velocity dependence of friction only on the branch of the $\mu(v)$ curve where the friction coefficient increases with increasing speed. For the studied cases, the friction coefficient is very weakly velocity-dependent. Sometimes unstable sliding occurs, resulting in a sliding speed that fluctuates over time. The average sliding speed in our studies was ~ 3 mm/s.

To study the velocity and pressure dependence of the wear rate, we slid the metal plate-block system on the tested surfaces for different distances: 21.5 cm on tile, 18 cm on sandpaper, and 10 cm on polished steel. The wear rate was determined from the mass change, defined as the difference in the mass of the plate-block system before and after sliding, using a high-precision balance (Mettler Toledo analytical balance, model MS104TS/00) with a sensitivity of 0.1 mg. After each sliding sequence, the surface was cleaned using a brush or a single-use non-woven fabric.

The surface roughness of all surfaces used in this study was measured using a Mitutoyo Portable Surface Roughness Measurement Surftest SJ-410. The instrument is equipped with a diamond tip with a radius of curvature of $R = 1$ μm and operates with a tip-substrate repulsive force of $F_N = 0.75$ mN. Measurements were taken with a step length (pixel) of 0.5 μm , a scan length of $L = 25$ mm, and a tip speed of $v = 50$ $\mu\text{m/s}$.

3 Experimental results

We have measured the wear rate and the friction force of PMMA and three types of glass blocks sliding on the tested surfaces. In all experiments, the normal load was $F_N = 104$ N, and the nominal contact area was $A_0 =$

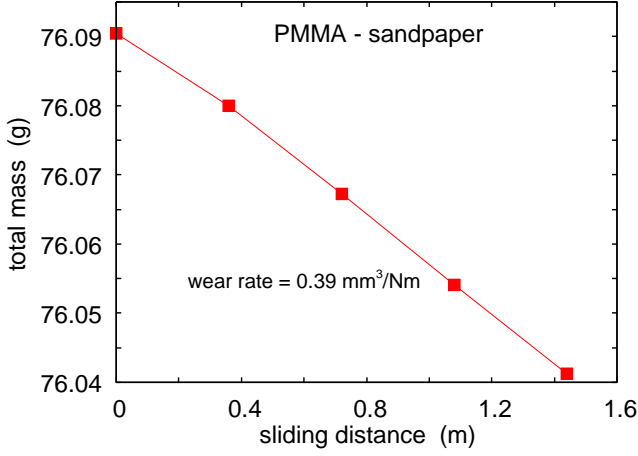


FIG. 3. The mass of the PMMA blocks and metal plate as a function of the sliding distance on the sandpaper P100 surface.

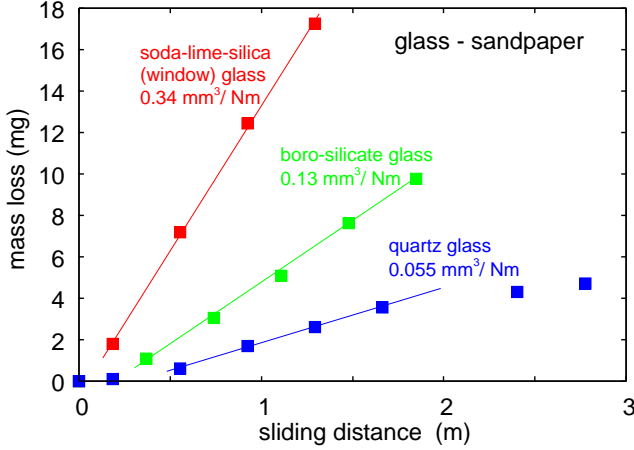


FIG. 4. The mass loss of blocks made of soda-lime glass (red), borosilicate glass (green), and quartz glass as a function of the sliding distance. The substrate used is sandpaper P100. The wear rates, $\Delta V/F_N L$, are indicated in the figure.

20 cm², resulting in a nominal contact pressure of $p_0 = 0.052$ MPa. Since PMMA, glass, ceramic tile, sandpaper, and polished steel are all relatively stiff materials, the blocks do not make uniform contact with the substrate surfaces at the macroscopic level. This non-uniformity is evident from the wear track patterns observed on the surface of blocks after a sliding act. As a result, the nominal contact pressure is not uniform but varies on the length scale of the block dimensions.

Fig. 2 shows the mass of the PMMA blocks and metal plate as a function of the sliding distance for the tile surface. Experiments performed on two consecutive days gave different results: on the first day, the wear rate was $\Delta V/F_N L = 0.021$ mm³/Nm, while on the second day, it was 0.010 mm³/Nm. Here, we calculated the wear volume from the mass loss, assuming a PMMA mass density

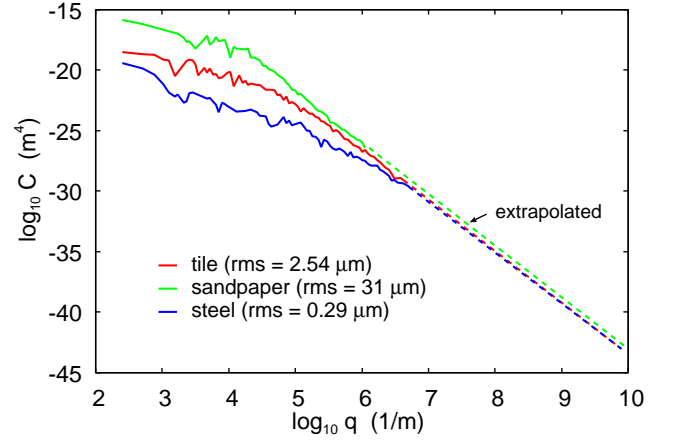


FIG. 5. The surface roughness power spectra of the tile, steel and sandpaper surfaces used in the wear studies. The dotted regions are extrapolated with a slope corresponding to the Hurst exponent $H \approx 1$.

of $\rho = 1180$ kg/m³. In both measurements, the wear rate was proportional to the sliding distance, suggesting that the difference in wear rate between the two days must be due to changes in external conditions (e.g., humidity, which was not measured) or some aging process that altered the properties of the worn PMMA or tile surface. We did not observe any PMMA particles adhering to the tile surface, but we cannot exclude the possibility that the tile surface asperities were covered by a nanometer-thin film of PMMA.

For PMMA on the sandpaper P100 surface, a significantly higher wear rate was observed, with $\Delta V/F_N L = 0.39$ mm³/Nm. In contrast, for the polished steel surface, no mass change was detected after a sliding distance of 4 m. However, given that the resolution of the measuring instrument was 0.1 mg, it is possible that a smaller amount of wear may have occurred but was below the detection limit.

The wear produced a white powder consisting of PMMA particles, which was easily brushed away after each sliding act. The PMMA wear particles were transparent, and the optical method available to us did not provide sufficient contrast. As a result, we were unable to analyze the size of the PMMA wear particles using the same optical microscope that was used for rubber wear particles in Ref. [1].

The wear rate for glass blocks sliding on sandpaper P100 surfaces is shown in Fig. 4. The figure presents the mass loss of blocks made of soda-lime (red), borosilicate (green), and quartz glass as a function of the sliding distance. The corresponding wear rates, given by $\Delta V/F_N L = 0.34, 0.13$, and 0.055 mm³/Nm for the three glass types, respectively, were calculated using assumed mass densities of $\rho = 2440, 2230$, and 2200 kg/m³ for

soda-lime, borosilicate, and quartz glass, respectively. As in the case of PMMA, we were unable to analyze the wear particles using optical methods due to their transparency and equipment limitations.

Fig. 5 shows the surface roughness power spectra of the tile, sandpaper, and steel surfaces used in the wear studies. The dotted regions represent extrapolated portions with a slope corresponding to a Hurst exponent of $H \approx 1$. Both the tile and steel surfaces are harder and elastically stiffer than PMMA, and are therefore treated as rigid with no deformation of their surface roughness profiles. The sandpaper surface consists of very hard corundum (aluminum oxide) particles, which can also be considered rigid when in contact with PMMA and even with glass surfaces. (The penetration hardness of corundum is approximately 30 GPa, compared to about 15 GPa for quartz.)

However, the corundum particles are embedded in a polymer fiber mat that contains an acrylic resin (see Fig. 6), which is elastically and plastically much softer than glass and likely similar in properties to PMMA. When sandpaper is pressed against silica glass surfaces, surface roughness components with wavelengths longer than the size of the corundum particles (diameter $D \approx 160 \mu\text{m}$ for P100 sandpaper; see Fig. 6) are easily flattened. These long-wavelength components should not be included in wear rate calculations for silica glass surfaces if the substrate is treated as rigid. For this reason, we exclude the roughness components with wavenumbers $q < 2\pi/D \approx 4 \times 10^4 \text{ m}^{-1}$ from the power spectrum of the sandpaper surface (green line in Fig. 5) when calculating wear rates for glass surfaces. For PMMA on sandpaper, it is less clear whether this same power spectrum correction is necessary. However, for consistency, we apply the same long-wavelength cut-off for PMMA in the present study.

In this study, we neglected the surface roughness of the PMMA and glass surfaces because, in all cases, it was much smaller than that of the hard countersurfaces.

4 Theory of sliding wear

Sliding wear depends on the size of the contact regions and on the stress acting within these regions [18]. The theoretical model used in this study follows the approach introduced in Ref. [1] for rubber wear. Here, we present an alternative derivation of the main result, which is also extended to include plasticity effects relevant to PMMA/glass sliding contacts.

Cracks at the surface of a solid can be induced by both the normal and the tangential stress acting on the surface, but particle removal is caused mainly by the tangential stress. Let $\tau = \tau(\zeta_r)$ be the effective shear stress acting in an asperity contact region with a radius r_0 .

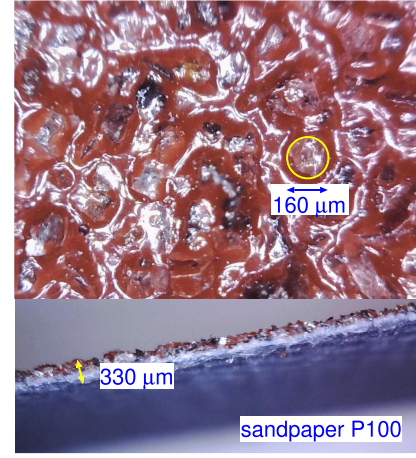


FIG. 6. Top: Picture of sandpaper P100. The corundum particles have an average diameter of $\approx 160 \mu\text{m}$. Bottom: Cross-section of the sandpaper. The sandpaper P100 has a thickness of $\approx 330 \mu\text{m}$.

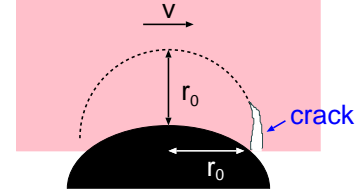


FIG. 7. A PMMA block sliding in contact with a hard countersurface. The sliding speed v and the radius of the contact region r_0 are indicated. The deformation field extends into the polymer a similar distance as it extends laterally.

The magnification ζ_r is determined by the radius of the contact region, $q_r = \pi/r_0$, $\zeta_r = q_r/q_0$. The elastic energy stored in the deformed asperity contact is (see Fig. 7)

$$U_{\text{el}} \approx \frac{\tau^2}{E^*} r_0^3,$$

where the effective modulus $E^* = E/(1 - \nu^2)$ (we assume that the substrate is rigid). More accurately, assume that the shear stress acts uniformly within a circular region with a radius r_0 . The center of the circular region will displace a distance u given by $ku = F$, where $F = \pi \tau r_0^2$ is the force and $k \approx (\pi/2)E^*r_0$ the spring constant. This gives the elastic energy

$$U_{\text{el}} = \frac{1}{2} k u^2 = \frac{F^2}{2k} = \frac{(\pi r_0^2 \tau)^2}{\pi E^* r_0} = \pi \frac{\tau^2}{E^*} r_0^3. \quad (1)$$

In order for the shear stress to remove a particle of linear size r_0 , the stored elastic energy must be larger than the fracture (crack) energy, which is of the order

$$U_{\text{cr}} \approx \gamma 2\pi r_0^2, \quad (2)$$

where γ is the energy per unit surface area to break the bonds at the crack tip. If $U_{\text{el}} > U_{\text{cr}}$, the elastic energy is large enough to propagate a crack and remove

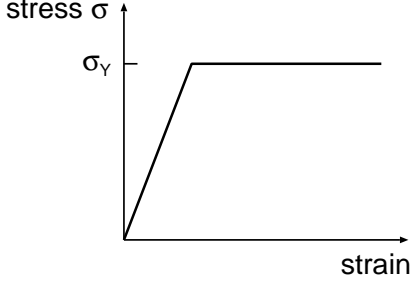


FIG. 8. The relation between the stress and the strain in elongation for the simplest elastoplastic model assumes that the maximum stress equals the yield stress, σ_Y . The penetration hardness is typically $\sigma_P \approx 3\sigma_Y$, where σ_P represents the ratio between the indentation force and the indentation cross-sectional area.

a particle[4–6]. Thus, for a particle to be removed, we must have $\tau > \tau_c$, where

$$\tau_c = \beta \left(\frac{2E^*\gamma}{r_0} \right)^{1/2}, \quad (3)$$

where β is a number of order unity, which takes into account that the wear particles, in general, are not hemispherical as assumed above.

In what follows, we will treat the polymer surface as smooth and assume only roughness on the counter surface. We will denote a substrate asperity, where the shear stress is high enough to remove a particle of size r_0 , as a *wear-asperity*, and the corresponding contact region as the *wear-contact region*.

If we assume that during sliding, the effective shear stress τ is proportional to the normal stress σ , $\tau = \mu\sigma$, we find that particles will be removed only if the contact stress $\sigma > \sigma_c(\zeta)$, where

$$\sigma_c = \frac{\beta}{\mu} \left(\frac{2E^*\gamma}{r_0} \right)^{1/2}. \quad (4)$$

For randomly rough surfaces, for elastic contact the probability distribution of contact stress equals:

$$P(\sigma, \zeta) = \frac{1}{(4\pi G)^{1/2}} \left(e^{-(\sigma-\sigma_0)^2/4G} - e^{-(\sigma+\sigma_0)^2/4G} \right), \quad (5)$$

where σ_0 is the nominal (applied) pressure and where

$$G = \frac{\pi}{4} (E^*)^2 \int_{q_0}^{\zeta q_0} dq q^3 C(q), \quad (6)$$

where $C(q)$ is the surface roughness power spectrum.

When the stress in the asperity contact region becomes high enough, plastic flow occurs. In the simplest model, it is assumed that a material deforms as a linear elastic solid until the stress reaches a critical level, the so-called

plastic yield stress, where it flows without strain hardening (see Fig. 8). The yield stress in elongation is denoted by σ_Y . In indentation experiments, where a sharp tip or a sphere is pushed against a flat solid surface, the penetration hardness σ_P is defined as the ratio between the normal force and the projected (on the surface plane) area of the plastically deformed indentation. Typically, $\sigma_P \approx 3\sigma_Y$. We note that the yield stress of materials often depends on the length scale (or magnification) which in principle can be included in the formalism we use [20, 21].

The influence of plastic flow on the contact mechanics can be taken into account in the Persson contact mechanics approach by replacing the boundary condition $P(\infty, \zeta) = 0$ with the condition that there is no stress at the interface above the penetration hardness, i.e., $P(\sigma, \zeta) = 0$ for $\sigma > \sigma_P$. Thus, the maximum stress at the interface is equal to the penetration hardness σ_P . This approach is based on the simplest elastoplastic description, where only elastic deformation occurs for $\sigma < \sigma_P$, while for $\sigma = \sigma_P$, the material flows without work-hardening so that the maximal stress equals σ_P (see Fig. 8). The pressure probability distribution for this case is given by[19]:

$$P(\sigma, \zeta) = \frac{2}{\sigma_P} \sum_{n=1}^{\infty} \sin(s_n \sigma_0) \sin(s_n \sigma) e^{-s_n^2 G(\zeta)} + P_{pl}(\zeta) \delta(\sigma - \sigma_P) \quad (7)$$

where $s_n = n\pi/\sigma_P$ and

$$P_{pl} = \frac{\sigma_0}{\sigma_P} + \frac{2}{\pi} \sum_{n=1}^{\infty} \frac{(-1)^n}{n} \sin(s_n \sigma_0) e^{-s_n^2 G(\zeta)} \quad (8)$$

As $\sigma_P \rightarrow \infty$, (7) reduces to (5). The $P(\sigma, \zeta)$ is also the pressure distribution resulting from *elastic* deformations if the two surfaces are separated and brought into contact again at the same position. Hence, it is the pressure distribution that should be used to obtain the elastic energy, which enters into the theory of the wear rate.

In Fig. 9, we show $P(\sigma, \zeta)$ as a function of the stress σ for $\zeta = 1857$ for PMMA in contact with the tile surface, with the power spectrum given by the red curve in Fig. 5. The tile surface is considered as rigid and the PMMA elastic (green curve) or elastoplastic (red curve) with the penetration hardness $\sigma_P = 0.4$ GPa.

When the interface is studied at the magnification ζ , the area $A = A_{wear}(\zeta)$, where the shear stress is high enough to remove particles, is given by

$$\frac{A_{wear}(\zeta)}{A_0} = \int_{\sigma_c(\zeta)}^{\infty} d\sigma P(\sigma, \zeta). \quad (9)$$

When we study the interface at the magnification ζ , the smallest wear particles observed have the size $r_0 \approx \pi/q_r$,

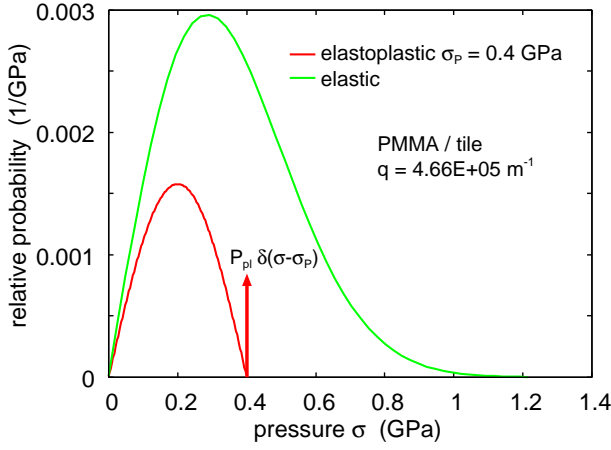


FIG. 9. The stress probability distribution $P(\sigma, \zeta)$ as a function of the stress σ for PMMA in contact with the tile surface, with the power spectrum given by the red curve in Fig. 5. The magnification $\zeta = q/q_0$, with $q = 4.66 \times 10^5 \text{ m}^{-1}$ and $q_0 = 251 \text{ m}^{-1}$. The tile surface is considered as rigid and the PMMA as elastic (green curve) with $E = 3 \text{ GPa}$ and $\nu = 0.3$, or elastoplastic (red curve) with $\sigma_P = 0.4 \text{ GPa}$.

with $q_r = \zeta q_0$. We may say that at the magnification ζ , there is a pixel size of $r_0 = \pi/\zeta q_0$, and the smallest removed particle, which can be observed at this magnification, is determined by the pixel size. As previously stated, such a particle can be removed from the polymer surface if $U_{el} > U_{cr}$, where U_{el} is the stored elastic energy ($\sim r_0^3$) in a volume element of linear size r_0 , and U_{cr} is the energy needed to break the bonds and detach the particle. $U_{cr} \approx \gamma 2\pi r_0^2$, where γ is the energy per unit surface area to propagate the crack. The crack energy γ depends on the speed of bond-breaking and will take a range of values, $\gamma_0 < \gamma < \gamma_1$. The faster the crack propagates, the larger γ becomes. The smallest stored elastic energy $U_{el} = U_{el0}$, which can remove a particle, is given by $U_{el0} \approx \gamma_0 2\pi r_0^2$, but for this case, the crack moves extremely slowly, and the incremental displacement Δx during the interaction between the (moving) *wear-asperity* and the crack is very small, requiring many $\sim r_0/\Delta x$ contacts to remove the particle. If the interaction with a *wear-asperity* results in $U_{el} \gg U_{el0}$, the crack will move much faster (Δx is much bigger), and far fewer contacts are needed to remove a particle. During sliding, the crack will be in contact with many *wear-asperities* of different sizes, so it will experience a wide range of crack-tip movements Δx before the particle is finally removed.

The probability that the stress at an arbitrary point on the polymer surface is between σ and $\sigma + d\sigma$, when the interface is studied at the magnification ζ , is given by $P(\sigma, \zeta)d\sigma$. If $\sigma > \sigma_c$, the local stress results in $U_{el} > U_{el0}$, so in principle, a particle could be removed. But during the interaction time, the crack moves only the distance $\Delta x(\gamma)$, where we assume the relevant γ is given by $U_{el} =$

γr_0^2 . Hence, $N(\gamma) = r_0/\Delta x$ contacts are needed to remove the particles. Thus, after the run-in, the probability that a particle will be removed from the regions where the stress is in the range σ to $\sigma + d\sigma$ will be $P(\sigma, \zeta)d\sigma/N(\gamma)$. The total probability will be

$$P^* = \int_{\sigma_c}^{\infty} d\sigma \frac{P(\sigma, \zeta)}{1 + r_0(\zeta)/\Delta x(\sigma, \zeta)} \quad (10)$$

where we have added 1 in the denominator in order for the limit $\Delta x/r_0 \rightarrow \infty$ to be correct. In (10), the cut-off stress σ_0 is determined by $U_{el} = U_{el0}$. There are $N^* = A_0/\pi r_0^2$ pixels on the surface, so sliding the distance $L = 2r_0$ will result in removing N^*P^* particles, corresponding to the volume $V = (2\pi r_0^3/3)N^*P^*$. Thus, we get $V/L = (\pi r_0^2/3)N^*P^*$ or $V/LA_0 = P^*/3$. Using (10), this gives

$$\frac{V}{LA_0} = \frac{1}{3} \int_{\sigma_c}^{\infty} d\sigma \frac{P(\sigma, \zeta)}{1 + r_0(\zeta)/\Delta x(\sigma, \zeta)} \quad (11)$$

which is the same as (17) in Ref. [1], except that the factor of 1/2 in (17) in Ref. [1] is replaced by 1/3 in (10) due to a slightly different description of the particle removal process. Eq. (11) shows that the wear volume per unit sliding length is proportional to the nominal surface area, as expected when the nominal contact pressure is constant.

The number of contacts needed to remove a particle $N_{\text{cont}} \approx r_0/\Delta x$ depends on the crack energy γ , but it could be a large number (10^2 or more) if the macroscopic relation between the tear-energy γ and Δx would also hold at the length scale of the wear particles.

The theory above estimates the wear volume by considering particles of a specific size characterized by radius r_0 . At the magnification level $\zeta = q_r/q_0 = \pi/q_0 r_0$, these correspond to the smallest observable wear particles. To obtain the total wear volume, contributions from all relevant length scales must be accumulated as the magnification increases. To avoid double-counting of similarly sized particles, the magnification is incremented in steps of approximately a factor of 2, expressed as $\zeta = 2^n = \zeta_n$, where $n = 0, 1, \dots, n_1$ and $2^{n_1} q_0 = q_1$. Each range between $\zeta = 2^n$ and 2^{n+1} is referred to as a two-interval. Using

$$\sum_{n=0}^{n_1} f_n \approx \int_0^{n_1} dn f_n = \frac{1}{\ln 2} \int_1^{\zeta_1} d\zeta \frac{1}{\zeta} f(\zeta),$$

we can write the total wear volume when Δx is constant as

$$\begin{aligned} \frac{V}{A_0 L} &\approx \frac{1}{3} \sum_{n=0}^{n_1} \frac{1}{1 + r_0(\zeta_n)/\Delta x} \frac{A_{\text{wear}}(\zeta_n)}{A_0} \\ &\approx \frac{1}{3 \ln 2} \int_1^{\zeta_1} d\zeta \frac{1}{\zeta} \frac{1}{1 + r_0(\zeta)/\Delta x} \frac{A_{\text{wear}}(\zeta)}{A_0}. \end{aligned} \quad (12)$$

Using $\zeta r_0 = \pi/q_0$, this gives

$$\begin{aligned} \frac{V}{A_0 L} &\approx \frac{1}{3\ln 2} \int_1^{\zeta_1} d\zeta \frac{1}{\zeta + \pi/q_0 \Delta x} \frac{A_{\text{wear}}(\zeta)}{A_0} \\ &= \frac{1}{3\ln 2} \int_{q_0}^{q_1} dq \frac{1}{q + \pi/\Delta x} \frac{A_{\text{wear}}(q)}{A_0}. \end{aligned} \quad (13)$$

When Δx depends on γ , we get

$$\frac{V}{A_0 L} = \frac{1}{3\ln 2} \int_{q_0}^{q_1} dq \int_{\sigma_c(\zeta)}^{\infty} d\sigma \frac{P(\sigma, \zeta)}{q + \pi/\Delta x(\sigma, \zeta)}, \quad (14)$$

where $\zeta = q/q_0$. It is convenient to write $q = q_0 e^\xi$, so that $dq = q d\xi$, and

$$\frac{V}{A_0 L} = \frac{1}{3\ln 2} \int_0^{\xi_1} d\xi \int_{\sigma_c(\zeta)}^{\infty} d\sigma \frac{P(\sigma, \zeta)}{1 + r_0(\zeta)/\Delta x(\sigma, \zeta)}. \quad (15)$$

where $\xi_1 = \ln(q_1/q_0)$.

If we write

$$Q(\sigma, \zeta) = \frac{P(\sigma, \zeta)}{1 + r_0(\zeta)/\Delta x(\sigma, \zeta)}$$

we can define the average number of contacts needed to remove a particle of size $r_0 = \pi/\zeta q_0$ as

$$\langle N_{\text{cont}} \rangle = \frac{\int_{\sigma_c(\zeta)}^{\infty} d\sigma N_{\text{cont}}(\sigma, \zeta) Q(\sigma, \zeta)}{\int_{\sigma_c(\zeta)}^{\infty} d\sigma Q(\sigma, \zeta)} \quad (16)$$

where

$$N_{\text{cont}}(\sigma, \zeta) = 1 + r_0(\zeta)/\Delta x(\sigma, \zeta).$$

The distribution of particles of different sizes is given by (17) [or (18)]. Thus, the number of particles with radius r_0 between $(\pi/q_0)2^{-n-1/2}$ and $(\pi/q_0)2^{-n+1/2}$ is

$$\frac{N_n}{A_0 L} \approx \frac{1}{3\pi r_0^3(\zeta_n)[1 + r_0(\zeta_n)/\Delta x]} \frac{A_{\text{wear}}(\zeta_n)}{A_0} \quad (17)$$

or, when Δx depends on γ ,

$$\frac{N_n}{A_0 L} \approx \frac{1}{3\pi r_0^3(\zeta_n)} \int_{\sigma_c(\zeta_n)}^{\infty} d\sigma \frac{P(\sigma, \zeta_n)}{1 + r_0(\zeta_n)/\Delta x(\sigma, \zeta_n)}. \quad (18)$$

The theory presented above assumes that all length scales contribute independently to the wear rate. This cannot be strictly true since a long crack, which would result in a large wear particle, will change the stress field in its vicinity out to a distance of the order of the length of the crack. This effect, known as crack shielding, reduces the ability for smaller cracks to grow in the neighborhood of longer cracks. However, crack tip shielding is much weaker for sliding contacts as compared to polymer strips elongated by uniform far-field stress.

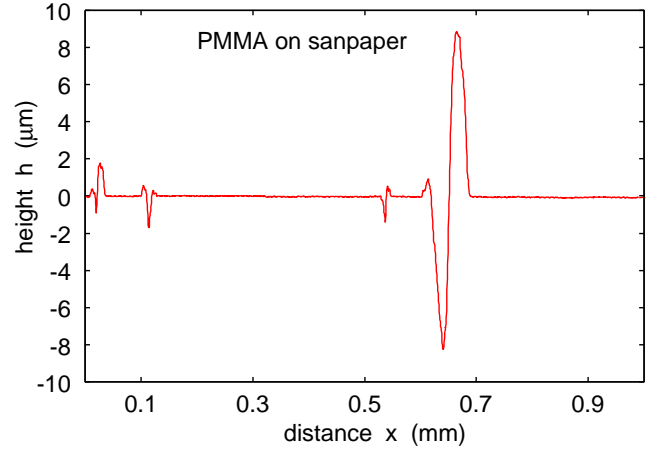


FIG. 10. The height profile orthogonal to the ploughing tracks after a PMMA block was slid a short distance on a sandpaper P100 surface.

Note that if $r_0/\Delta x$ is large, a long run-in distance would be needed before the wear reaches a steady state. This is particularly true if the nominal contact pressure is small, where the distance between the wear asperity contact regions may be large. However, since the contact regions within the macroasperity contacts are densely distributed and independent of the nominal contact pressure, there may, in some cases, be enough wear asperity contact regions within the macroasperity contact regions to reach the N_{cont} needed for wear particle formation even over a short sliding distance.

5 Role of plastic flow

In the context of sliding wear, asperity contact regions may deform plastically at short length scales even when brittle fracture dominates at longer scales[6, 7, 9]. This phenomenon has been observed even in very brittle materials such as silicon nitride. The tendency for plastic flow rather than crack propagation at small length scales can be understood based on the Griffith fracture criterion [4–6, 22]: to remove a particle of linear size r_0 , the local stress must be high enough that the stored elastic energy in a volume element $\sim r_0^3$ exceeds the fracture energy $\sim \gamma r_0^2$. This leads to the condition $\sigma > \sigma_c$, where σ_c is defined by Eq. (4), for the removal of a particle. However, if σ_c exceeds the penetration hardness σ_P at the length scale r_0 , crack propagation cannot occur, and the material will instead flow plastically.

This principle is exploited in *ductile mode cutting*, in which material is removed by plastic flow instead of brittle fracture, producing a smoother surface with minimal damage [23, 24]. For example, when a hard asperity such as a diamond tip slides across the surface of a brittle solid at sufficiently low load (so that the contact region is very small), the material may be removed by cutting (pro-

ducing micro or nano chips through plastic deformation) without the formation of surface cracks. This technique is commonly used to machine brittle materials such as silica glass, silicon, silicon nitride, or tungsten carbide [23, 24]. Cutting in this context refers to the removal of material from the surface in the form of primary debris or microchips, with minimal lateral displacement, resembling conventional machining.

In many situations, plastic flow does not result in material removal but only in its displacement [10, 11]. When the slopes of asperities are not too steep and the sliding friction is small, ploughing tracks are formed. In such cases, the stress in the asperity contact regions is mainly compressive, which suppresses the formation of cracks, and the material is displaced to the sides of the grooves by plastic flow rather than being detached as wear particles, a process more likely to occur for sharper surface features. The extent of the displaced material can be estimated from line scan topography measurements on an initially flat surface of the test material. If sliding occurs only once and at low contact pressure, the spacing between ploughing tracks is relatively large. We define the flat regions between the tracks as the *undeformed surface plane*. The volume of material removed as wear particles can be determined by comparing the material volumes below and above this undeformed surface plane.

To illustrate this, Fig. 10 shows a segment of a 10 mm long line scan for PMMA that was slid a short distance over a sandpaper surface. An analysis of the ploughing tracks from the entire scan indicates that most of the material volume removed below the undeformed surface plane was displaced rather than lost as wear particles. Such material displacement by plastic flow occur to some extent also for a brittle material like silica glass (see Appendix A).

In Fig. 11(a), we show the area of real contact as a function of the cut-off wavenumber q for PMMA on the tile surface. The cut-off wavenumber q corresponds to the shortest wavelength roughness included in the calculation and is related to the magnification ζ through $q = \zeta q_0$. In the calculations, we have used a penetration hardness of $\sigma_P = 0.4$ GPa for PMMA and assumed the tile surface to be rigid. When calculating the contact area for a given wavenumber $q = \zeta q_0$, only the long-wavelength roughness components with $q_0 < q < \zeta q_0$ are included. Note that all contact regions have yielded plastically when $q \approx 2 \times 10^6 \text{ m}^{-1}$, which corresponds to a wavelength of approximately $1 \text{ } \mu\text{m}$.

The sandpaper P100 surface exhibits a larger surface roughness power spectrum than the tile surface. For PMMA in contact with the sandpaper, plastic deformation begins at longer length scales, as shown in Fig. 11(b). For this surface, plastic yielding begins at $q \approx 10^4 \text{ m}^{-1}$, corresponding to a wavelength of approximately

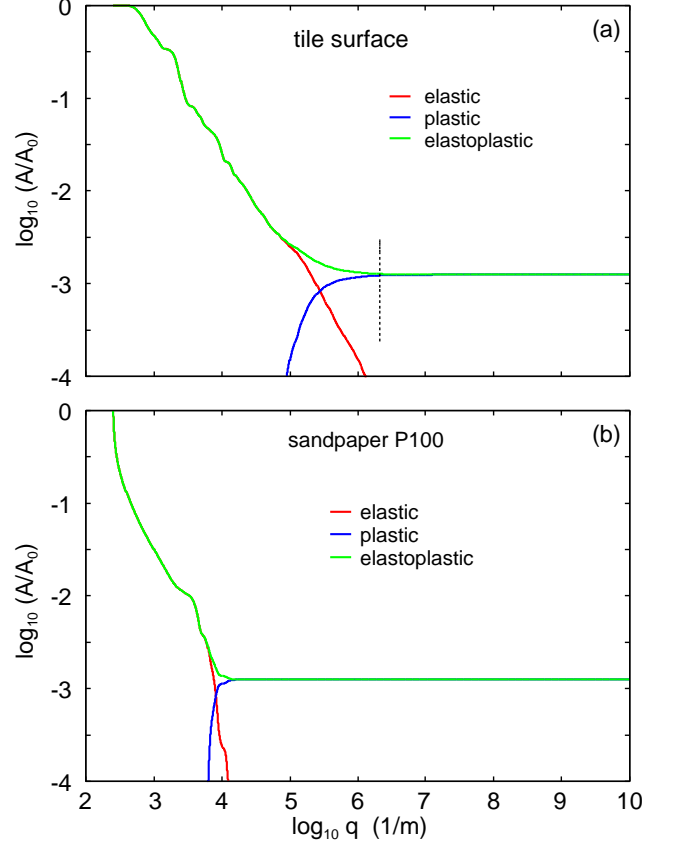


FIG. 11. The area of real contact as a function of the largest wavenumber q included in the calculation, for PMMA on the tile surface (a) and on the sandpaper P100 surface (b). The wavenumber q is related to the magnification ζ via $q = \zeta q_0$. The red and blue lines represent the elastic and plastic contact areas, respectively, and the green line indicates the elastic contact area for the elastoplastically deformed surface. The calculations assume elastoplastic contact with a Young's modulus of $E = 3$ GPa, a Poisson ratio of $\nu = 0.3$, and a penetration hardness of $\sigma_P = 0.4$ GPa.

0.3 mm, which is comparable to the average size of the sand particles.

The steel surface is relatively smooth. In this case, plastic deformation occurs only at very short length scales, involving surface roughness components with wavelengths below approximately 100 nm. These components are not significant for the wear process considered in this study. Therefore, for the steel surface, PMMA is treated as a purely elastic material.

6 Comparing theory with experiments

Here we compare the theoretical predictions for the wear rate with the experimental results for PMMA sliding on tile, sandpaper, and steel surfaces, as well as for silica glass sliding on the sandpaper surface.

PMMA on tile, sandpaper, and steel

We model PMMA as an elastoplastic material with a Young's modulus of $E = 3$ GPa and a Poisson ratio of $\nu = 0.3$. The penetration hardness of PMMA depends on the indentation time, as the deformation process is a stress-augmented, thermally activated flow. In this study, the indentation time is estimated as $\tau = r/v$, where v is the sliding speed and r is a characteristic length scale, approximately equal to the typical radius of a wear particle, $r \approx 3 \mu\text{m}$. For a sliding speed of $v \approx 3$ mm/s, the indentation time is estimated to be $\tau \approx 10^{-3}$ s.

For PMMA, the measured penetration hardness as a function of the strain rate is well described by the following empirical relation (in MPa) (see Ref. [25]):

$$\sigma_P \approx 0.313 + 0.0325 \log_{10}(\tau_0/\tau), \quad (20)$$

where $\tau_0 = 1$ s.

Using $\tau \approx 10^{-3}$ s, the penetration hardness is calculated as $\sigma_P \approx 0.41$ GPa.

The tile and steel surfaces have much higher elastic modulus and penetration hardness than PMMA and are therefore treated as rigid materials. The sandpaper consists of very hard and elastically stiff corundum (aluminum oxide) particles deposited on an elastically soft polymer film. As discussed in Sec. 3, this is accounted for by including only the substrate roughness components with wavenumber $q > 2\pi/D$, where D is the average diameter of the corundum particles. For the steel and tile surfaces, we use the surface roughness power spectra shown in Fig. 5. For the sandpaper, we exclude the region with $q < 2\pi/D$. In all cases, the measured power spectra are linearly extrapolated to larger wavenumbers on a log-log scale. The slope of the extrapolated region corresponds to a Hurst exponent $H \approx 1$, but the exact form of this extrapolation is not critical for the wear rate calculations presented below.

To calculate the wear rate, we need the relation between Δx and γ . This relationship has been experimentally studied for PMMA and varies slightly depending on the PMMA formulation[26]. The measured relation is well approximated by the following expression:

$$\begin{aligned} \Delta x &= 0, \quad \text{for } \gamma < \gamma_0, \\ \Delta x &= a (\sqrt{\gamma} - \sqrt{\gamma_0})^2 \left(\frac{\sqrt{\gamma} - \sqrt{\gamma_0}}{\sqrt{\gamma_1} - \sqrt{\gamma}} \right)^{\sqrt{\gamma_0/\gamma_1}} \end{aligned} \quad (21)$$

for $\gamma_0 < \gamma < \gamma_1$, where $\gamma_0 = 36.0$ J/m², $\gamma_1 = 517.0$ J/m², and $a = 5.3 \times 10^{-9}$ m³/J. Note that $\Delta x \rightarrow \infty$ as γ approaches γ_1 .

Using the power spectra shown in Fig. 5 and the relation between Δx and γ given by equation (21), we present in Fig. 12(a) the cumulative wear volume and in Fig. 12(b) the number of generated particles as functions of the logarithm of the particle radius for the PMMA-tile system.

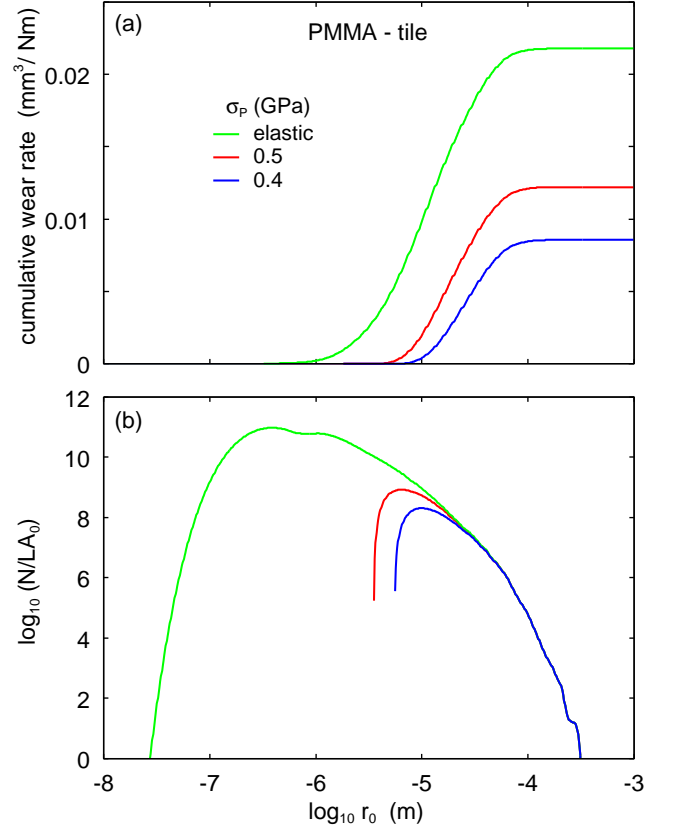


FIG. 12. (a) The cumulative wear volume and (b) the number of generated particles as functions of the logarithm of the particle radius for PMMA sliding on a tile surface. The wear rates without plastic deformation and with plastic deformation (assuming $\sigma_P = 0.4$ GPa, blue line) are approximately $0.22 \text{ mm}^3/\text{Nm}$ and $0.085 \text{ mm}^3/\text{Nm}$, respectively. The measured wear rate is approximately 0.1 to $0.2 \text{ mm}^3/\text{Nm}$. Calculations use $E = 3$ GPa, $\nu = 0.3$, and the measured relation between the crack-tip displacement $\Delta x(\gamma)$ and the tearing energy γ , shown in Fig. 13(a). The friction coefficient is $\mu = 0.5$, the nominal contact area $A_0 = 0.002 \text{ m}^2$, and the nominal contact pressure $\sigma_0 = 0.052 \text{ MPa}$, as in the experiment described in Sec. 3.

The green lines represent the results obtained without considering plastic deformation using equation (5), with the power spectrum indicated by the red line in Fig. 11. The red and blue lines correspond to calculations that include plasticity using equation (7).

The calculated wear rate for $\sigma_P = 0.4$ GPa [blue line in Fig. 12(a)] is $\Delta V/LF_N \approx 0.0085 \text{ mm}^3/\text{Nm}$, which is consistent with the experimental values (0.021 and 0.010 from two separate measurements; see Sec. 3). The peak in the number of generated particles in Fig. 12(b) occurs at particle sizes approximately one order of magnitude smaller than in previous studies of rubber wear. The optical method we used does not give sufficient contrast to accurately measure the PMMA particle sizes experimentally. The number of generated particles in different

size ranges can be determined from Fig. 12(b) using the two-interval separation method described previously.

The relationship between γ and Δx depends on the specific type of PMMA, but it generally follows the form given in equation (21), which is also depicted in Fig. 13(a). Note that Δx diverges as γ approaches the critical value γ_1 . In Fig. 13(b), we display the integrand of equation (15) for PMMA on the tile surface as a function of γ for all magnifications (or particle radii r_0), assuming no plastic flow (green lines) and including plasticity (red lines). Although the integration variable in equation (15) is pressure, each pressure value corresponds to a tearing energy as defined by equation (4). The red and green areas represent the superposition of many curves corresponding to various magnifications or particle radii.

Fig. 14(a) shows the cumulative wear volume and (b) the number of generated particles as functions of the logarithm of the particle radius for PMMA sliding on sandpaper. We have used the power spectrum of the sandpaper surface for $q > 2\pi/D$ and the measured friction coefficient $\mu = 0.60$. The green line is calculated using equation (5) without plasticity, and the red lines include plastic flow using equation (7). The wear rates without and with plastic deformation (with $\sigma_P = 0.4$ GPa) are approximately $1.74 \text{ mm}^3/\text{Nm}$ and $0.40 \text{ mm}^3/\text{Nm}$, respectively, while the measured wear rate is approximately $0.39 \text{ mm}^3/\text{Nm}$ (see Fig. 3).

For PMMA on the tile surface, several hundred contacts with wear asperities are required to remove a single PMMA wear particle. This is illustrated in Fig. 15(a), where the green line shows the effective number of contacts $\langle N_{\text{cont}} \rangle$ needed to detach a wear particle as a function of the logarithm of the wear particle radius. The red line in the figure, also shown in Fig. 12(a), represents the cumulative wear volume, including plastic deformation, as a function of the logarithm of the wear particle radius. Approximately 70 percent of the wear mass is attributed to particles removed in fewer than ~ 500 contacts with wear asperities.

For PMMA on the sandpaper surface, most wear particles are removed in a single contact between the PMMA and the corundum wear asperities. This is demonstrated in Fig. 15(b), where the sharp increase in cumulative wear volume occurs when $\langle N_{\text{cont}} \rangle \approx 0$, corresponding to the condition $\Delta x \gg r_0$.

Using the same parameters as above but with $\mu = 0.2$, for PMMA on the polished steel surface, and with the surface power spectrum shown in Fig. 5 (blue line), the predicted wear rate is $\Delta V/LF_N \approx 10^{-21} \text{ mm}^3/\text{Nm}$. This indicates negligible wear contribution from the considered mechanism. This prediction is consistent with our experimental findings, where no measurable wear was detected after sliding over a distance of 4 m on the steel

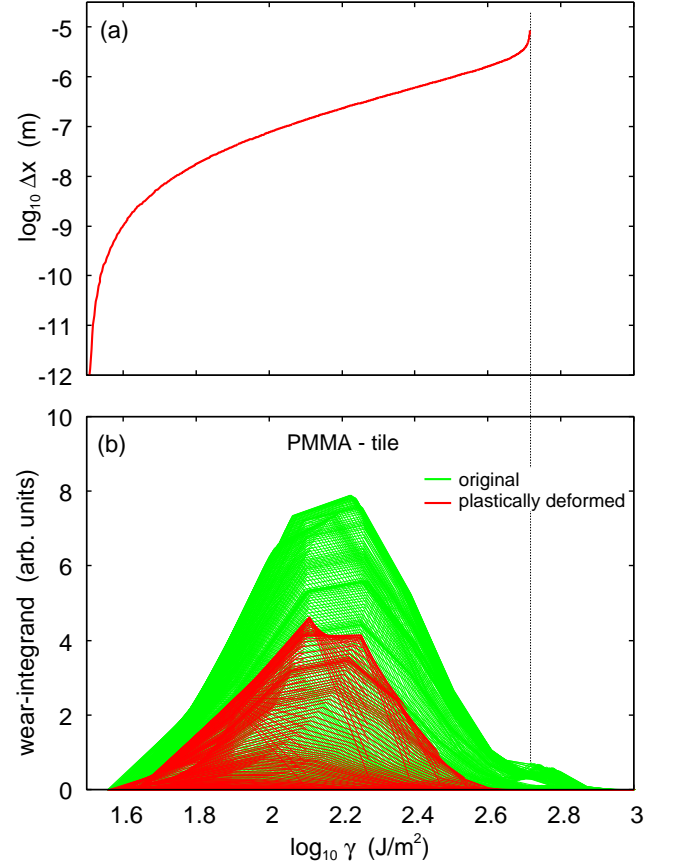


FIG. 13. (a) Relationship between the crack tip displacement per oscillation and the tearing (or crack) energy γ for PMMA, based on the measurements presented in Ref. [26]. (b) Integrand in equation (15) as a function of γ for all magnifications (or particle radii r_0), assuming elastic contact without plasticity (green lines) and elastoplastic contact with $\sigma_P = 0.4$ GPa (red lines).

surface. Given the resolution of our balance (0.1 mg), this corresponds to an experimental upper limit for the wear rate of approximately $10^{-4} \text{ mm}^3/\text{Nm}$.

Silica-lime, borosilicate and quartz glass on sandpaper

In Sec. 3, we studied the sliding wear of window glass (soda-lime), borosilicate glass, and quartz (crystalline SiO_2) on sandpaper. The sandpaper consists of corundum particles (crystalline Al_2O_3), which are both elastically stiffer and plastically harder than the glass materials, and are treated as rigid in our calculations. For silica glass and quartz, the Young's modulus is approximately $E \approx 70$ GPa, while for corundum it is approximately $E \approx 350$ GPa. The penetration hardness of corundum is $\sigma_P \approx 22$ GPa, which is higher than that of quartz, $\sigma_P \approx 12$ GPa (see Ref. [27]), borosilicate glass, $\sigma_P \approx 8$ GPa (see Ref. [28]), and soda-lime glass, $\sigma_P \approx 6$ –11 GPa (see Ref. [29]), depending on the loading

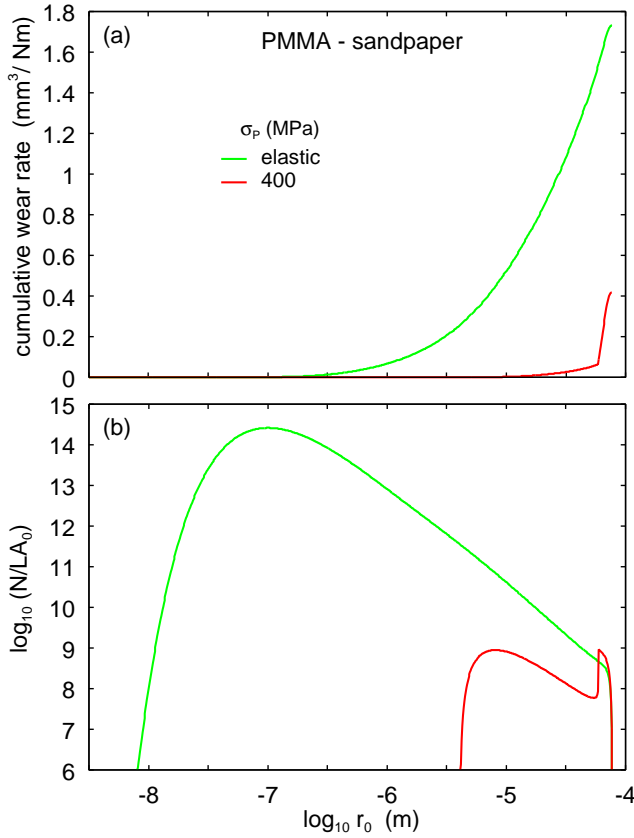


FIG. 14. (a) Cumulative wear volume and (b) number of generated particles as a function of the logarithm of the particle radius for PMMA on sandpaper P100. The wear rates without and with plastic deformation (assuming $\sigma_P = 0.4$ GPa) are approximately $1.74 \text{ mm}^3/\text{Nm}$ and $0.40 \text{ mm}^3/\text{Nm}$, respectively. The measured wear rate is approximately $0.39 \text{ mm}^3/\text{Nm}$ (see Fig. 3).

rate.

Fig. 16(a) shows the calculated cumulative wear volume, and Fig. 16(b) shows the number of wear particles, both as functions of the logarithm of the wear particle radius, for glass surfaces with different penetration hardness values sliding on sandpaper P100. The curve labeled “elastic” corresponds to infinite hardness, which implies no plastic deformation. The calculated wear rate for $\sigma_P = 10$ GPa is $\Delta V/LF_N \approx 0.33 \text{ mm}^3/\text{Nm}$, which is in close agreement with the experimentally measured wear rate for window glass ($0.34 \text{ mm}^3/\text{Nm}$; see Fig. 4).

However, the current theoretical model does not account for the observed reduction in wear rates for borosilicate glass and quartz, which are approximately 0.38 and 0.16 times smaller than the wear rate of window glass, respectively (see again Fig. 4).

7 Discussion

Many wear equations have been developed, but the most

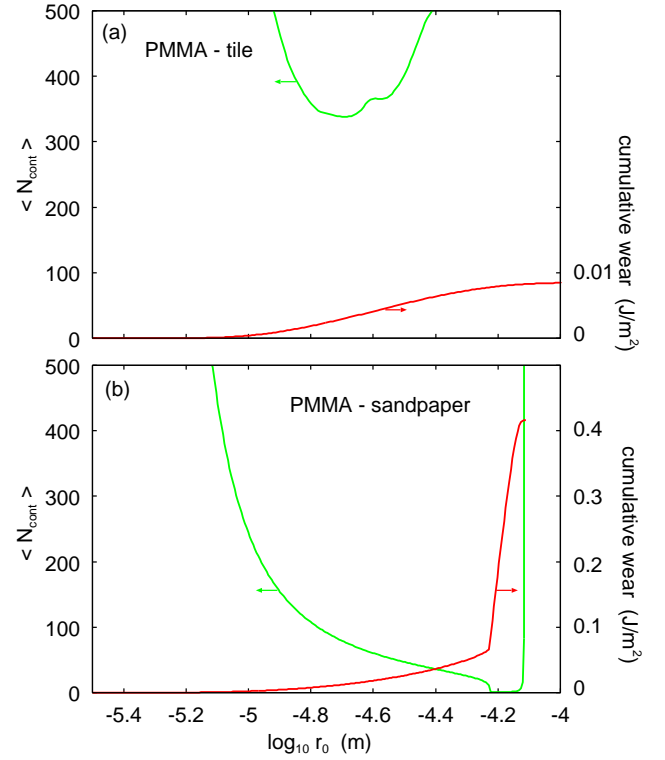


FIG. 15. Cumulative wear volume (red line) and the effective number of asperity contacts ($\langle N_{\text{cont}} \rangle$) required to remove a wear particle (green line) as functions of the logarithm of the wear particle radius. Results are shown for elastoplastic contact (assuming $\sigma_P = 0.4$ GPa) for PMMA on (a) the tile surface and (b) the sandpaper surface.

widely used is probably the Archard wear equation:

$$\frac{\Delta V}{LA_0} = K \frac{p_0}{\sigma_P} \quad (22)$$

where p_0 is the nominal contact pressure (assumed constant), and A_0 is the nominal contact area, related to the applied normal force via $F_N = p_0 A_0$. Equation (22) can also be written as

$$\frac{\Delta V}{F_N L} = \frac{K}{\sigma_P} \quad (23)$$

The parameter K is dimensionless but depends on the specific system under investigation, and it has been found to span a wide range of values.

Equation (23) assumes that all contact regions, when observed at the highest (atomic) resolution, have undergone plastic yielding, and that wear results from the removal of fragments of material from the area of real contact. However, this relation (with $K > 0$) cannot hold universally. If the elastic energy U_{el} stored in the contact regions is less than the critical energy U_{cr} on all relevant length scales, then no wear particles will form, even if the material has yielded plastically.

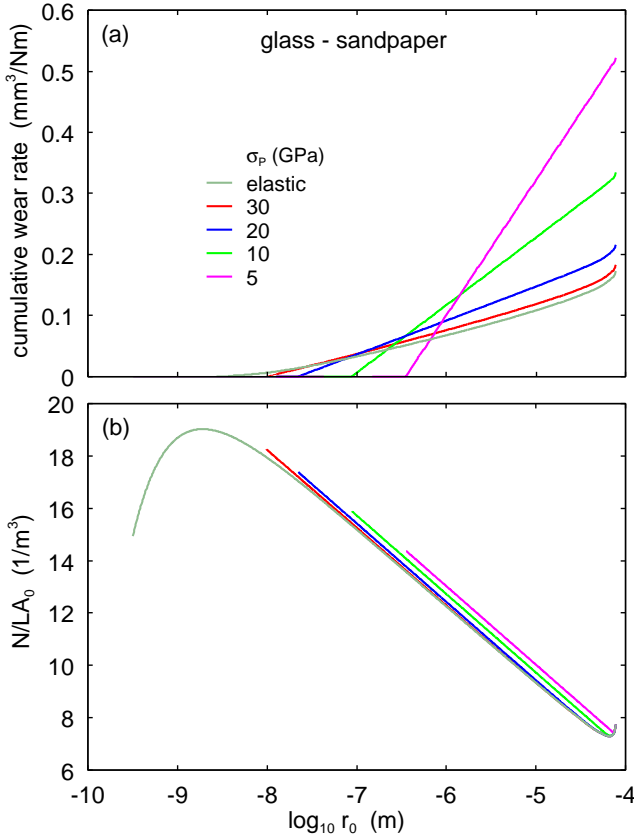


FIG. 16. (a) Cumulative wear volume and (b) number of wear particles as functions of the logarithm of the wear particle radius for glass sliding on sandpaper P100. Results are shown for different values of penetration hardness. The curve labeled “elastic” corresponds to infinite hardness, which implies no plastic deformation. The nominal contact area is $A_0 = 0.002 \text{ m}^2$ and the nominal contact pressure is $\sigma_0 = 0.052 \text{ MPa}$, as in the experiment described in Sec. 3. Calculations use $E = 70 \text{ GPa}$, $\nu = 0.3$, and a friction coefficient of $\mu = 0.34$.

Furthermore, even when wear does occur, Eq. (22) is generally not valid, even under the condition that all contact regions yield plastically. This point is illustrated in Fig. 17 for a hypothetical glass-sandpaper system.

Fig. 17 shows the calculated wear rate $\Delta V/F_N L$ (in mm^3/Nm) as a function of the penetration hardness σ_P for a glass surface sliding on the sandpaper P100 surface. The red and blue curves correspond to Young’s modulus $E = 70 \text{ GPa}$ and $E = 700 \text{ GPa}$, respectively, with $\nu = 0.3$ and $\mu = 0.34$. The dotted red and blue lines represent the wear rate under the assumption of purely elastic contact ($\sigma_P = \infty$).

For values of $\sigma_P > 2.5 \text{ GPa}$, the wear rate decreases with increasing σ_P , but at a slower rate than predicted by Eq. (22), which suggests a $1/\sigma_P$ scaling. Moreover, for small but non-zero values of σ_P , the wear rate tends toward zero. This result is expected because, at low σ_P , the

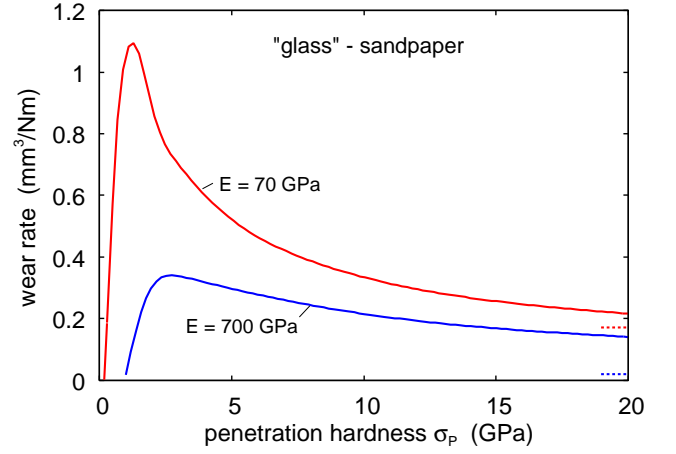


FIG. 17. The wear rate $\Delta V/F_N L$ (in mm^3/Nm) as a function of the penetration hardness for glass sliding on the sandpaper P100 surface. The red and blue curves correspond to Young’s modulus $E = 70 \text{ GPa}$ and $E = 700 \text{ GPa}$, respectively. In both cases, the Poisson ratio is $\nu = 0.3$ and the friction coefficient is $\mu = 0.34$. The dotted red and blue lines indicate the wear rates predicted under the assumption of purely elastic contact ($\sigma_P = \infty$).

interfacial stress is everywhere too small to generate wear particles. That is, the condition $U_{el} < U_{cr}$ is satisfied across all length scales considered.

In the study presented above, it was found that for PMMA sliding on the tile surface, the effective number of contacts N_{cont} required to detach a wear particle is much larger than unity. However, it is not clear whether, during relatively short sliding distances, points on the PMMA surface actually undergo contact with wear asperities as many times as expected from the large value of N_{cont} . This observation suggests that the relationship $\Delta x(\gamma)$ may need to be interpreted within a probabilistic framework, which will be discussed in the next section.

The Paris equation provides the crack-tip displacement Δx as a function of the tearing energy γ when a crack is subjected to oscillating strain or stress, such as those arising from external boundary forces acting on the solid. When γ is close to the fatigue limit γ_0 , a large number of oscillation cycles is required before the crack-tip displacement becomes measurable. It is commonly assumed that cracks propagate continuously with the number of stress cycles. However, in this study, we propose an alternative scenario.

We assume that when $\gamma < \gamma_1$, crack propagation occurs via stress-assisted thermally activated bond-breaking events. In this process, segments at the crack tip move in temporally irregular and discrete steps, each of which may be significantly larger than an atomic spacing. Therefore, if $U_{el} > U_{cr}$, the factor $1/(1 + r_0/\Delta x)$ may represent the probability of forming a wear particle during a

single contact event of size approximately r_0 , rather than the inverse of the number of contacts required to form such a particle. For example, if $\Delta x = 10^{-11}$ m per cycle (or less), which is expected when γ is sufficiently close to γ_0 , then during most stress cycles no significant crack advancement occurs. However, occasionally, a segment along the crack front may displace by a characteristic distance that exceeds atomic dimensions.

The wear process described above results from elastic energy that is temporarily stored in asperity contact regions during sliding. If this elastic energy on a given length scale r_0 exceeds the critical threshold $U_{el} > U_{cr}$, crack propagation may remove particles or fragments of size r_0 from the sliding surfaces. On the other hand, if the surface roughness is sufficiently small such that $U_{el} < U_{cr}$ across all asperity contact regions and on all relevant length scales, this wear mechanism will not occur.

This behavior is demonstrated in the case of PMMA sliding on a polished steel surface, where the predicted wear rate is $\Delta V/LF_N \approx 10^{-21}$ mm³/Nm. For comparison, on a tile surface with approximately ten times higher root-mean-square roughness (≈ 3 μ m compared to 0.3 μ m for the steel surface), the predicted wear rate is $\Delta V/LF_N \approx 0.01$ mm³/Nm. In general, there exists an abrupt transition in wear behavior: as surface roughness decreases, the system transitions from a regime of relatively high wear rates to one of extremely low wear.

This transition is illustrated in Fig. 18, which shows the logarithm of the wear rate as a function of the root-mean-square roughness h_{rms} , obtained by scaling the power spectrum of the tile surface. For smooth surfaces with small h_{rms} , no plastic flow occurs, and the elastoplastic results (blue line) are identical to those obtained under purely elastic conditions (green line). Similarly, a decrease in the friction coefficient reduces U_{el} . For the PMMA and tile system, numerical calculations show that when μ falls below approximately 0.15, the wear rate vanishes, as illustrated in Fig. 19.

Many studies have been conducted on UHMWPE sliding against very smooth counter surfaces, as these systems are of significant interest for artificial joint applications. The generation of wear debris has been identified as a major cause of failure in total joint replacements. In most of these systems, one of the bearing surfaces is made of a hard, extremely smooth metal or ceramic material, while the other surface consists of UHMWPE. Wear particles generated from UHMWPE during sliding can be released into the surrounding tissues, where they cause adverse cellular responses, potentially leading to bone resorption and implant loosening. Therefore, reducing the volume and number of UHMWPE wear particles is essential for improving the long-term clinical performance of total artificial joints.

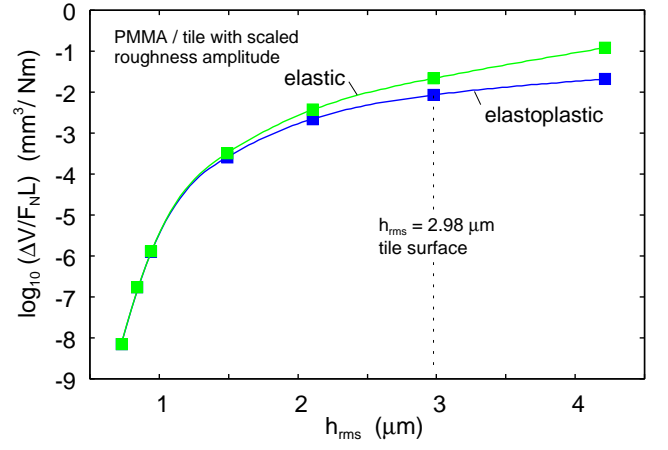


FIG. 18. The logarithm of the wear rate as a function of the root-mean-square roughness h_{rms} for PMMA in contact with a tile surface. The surface roughness is scaled to obtain different roughness amplitudes while maintaining the same fractal characteristics. The blue line represents the result for elastoplastic contact with a penetration hardness $\sigma_P = 0.4$ GPa, and the green line corresponds to purely elastic contact (no plastic deformation).

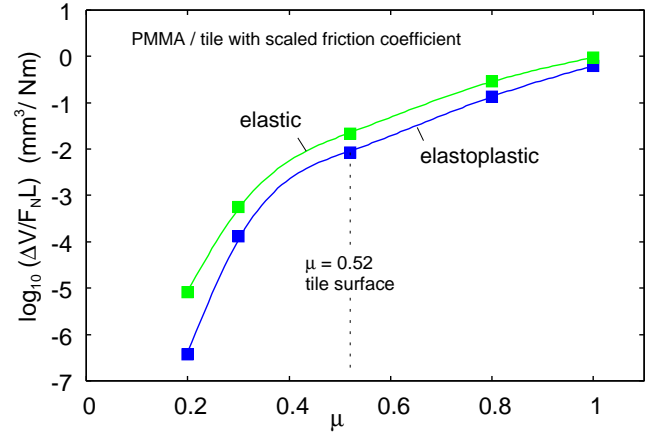


FIG. 19. The logarithm of the wear rate as a function of the friction coefficient for PMMA in contact with a tile surface. The friction coefficient is varied from the experimentally measured value of 0.52 to both lower and higher values. The blue line shows the result for elastoplastic contact with a penetration hardness $\sigma_P = 0.4$ GPa, and the green line shows the result for elastic contact (without plastic deformation).

In typical artificial joint systems, the counter surface in contact with the UHMWPE has an rms roughness below 0.03 μ m. For such smooth surfaces, the wear mechanism described earlier cannot occur, and the observed wear rate is typically very low, on the order of 10^{-8} mm³/Nm. The most probable origin of this wear is polymer asperity wear. The UHMWPE surfaces in these systems often exhibit surface roughness with amplitudes on the order of micrometers (rms roughness of approximately 1 μ m). Under load, many of these asperities undergo elastoplas-

tic deformation. During sliding, tensile stresses can develop at the base of the asperities, particularly on their trailing edges, which may lead to crack propagation or stress corrosion and the formation of wear particles. This mechanism likely dominates wear in artificial joints and in other cases where polymers slide against very smooth surfaces.

The wear process discussed above is not the only possible mechanism but is expected to be dominant unless the counter surface roughness is extremely small. In such cases, significantly lower wear rates are expected compared to those for rougher surfaces such as tile or sandpaper.

Another important wear mechanism is adhesive wear, which is particularly relevant for metals [30]. In asperity contact regions, local pressures can exceed the strength of the native oxide layer present on most metals, leading to direct metal-to-metal contact. If the materials are similar in composition, such as steel sliding on steel, cold-welded junctions can form and result in material transfer. This phenomenon has been confirmed in experiments using radioactive tracers to monitor material exchange.

The transferred material typically includes fragments of the oxide layer, and the exposed fresh metal quickly oxidizes, forming a new transferred film enriched with oxides. This film is often more weakly bound to the substrate than the bulk metal, and after sufficient sliding, oxide-rich particles may be generated. These particles may initially remain trapped between the surfaces, but over time they detach and contribute to the wear debris.

8 Summary and conclusion

We have presented experimental data for the wear rate of polymethyl methacrylate (PMMA) sliding on a tile surface, on sandpaper, and on a polished steel surface, as well as for soda-lime, borosilicate, and quartz glass sliding on sandpaper. A recently developed theory of rubber wear [1] has been extended to include the effects of plastic deformation. The experimental results were compared with the theoretical predictions. We find generally good agreement between them; however, two unresolved issues remain:

(a) The theory predicts similar wear rates for window (soda-lime-silica) glass and quartz (crystalline SiO_2), as both materials exhibit nearly identical elastic modulus and penetration hardness. Experimentally, however, the wear rate for quartz is approximately 0.16 times that of window glass. This discrepancy may be attributed to the structural differences between amorphous and crystalline materials. In crystalline solids such as quartz, plasticity occurs primarily through the generation and motion of dislocations, whereas in amorphous materials like window glass, plastic deformation is governed by local atomic

rearrangements within nanometer-sized domains. These distinct deformation mechanisms may result in differences in work-hardening behavior and flow properties, which are not captured by the simplified elastoplastic model used in this study.

(b) For PMMA sliding on the tile surface, the theoretical model predicts that the removal of a single wear particle requires a large number (on the order of a few hundred) of asperity contacts. Due to the relatively short sliding distances employed in the experiments, it is unclear whether such a number of contacts actually occurred. As discussed in the main text, this suggests that the relationship between the tearing energy γ and the crack tip displacement Δx (i.e., the Paris curve) may require reinterpretation. In particular, crack propagation may not proceed in a continuous manner but may instead occur through stochastic, thermally assisted bond-breaking events. In this scenario, the crack tip may undergo finite, and potentially large, displacements in some asperity contacts, while in others no propagation occurs.

Paris curves are usually measured for relatively large, macroscopic samples (approximately 1 cm in length), whereas wear typically involves the removal of micrometer-sized particles through crack propagation. Measuring the $\Delta x(\gamma)$ relationship for micrometer-sized cracks is an important objective for improving our understanding of wear processes.

Acknowledgments: We thank M. Ciavarella for useful discussions.

Author declarations: The authors have no conflicts to disclose. All authors have contributed equally.

Data availability: The data that support the findings of this study are available within the article. The data that support the findings of this study is available from the corresponding author upon reasonable request.

Appendix A We have studied the ploughing tracks on a soda-lime glass block (a), a borosilicate glass block (b), and a quartz block (c) after they were slid a short distance on a sandpaper P100 surface (see Fig. 20). Even for these brittle materials, some of the material removed from below the undeformed surface plane is displaced by plastic flow to regions above the undeformed surface plane.

-
- [1] B. N. J. Persson, R. Xu, N. Miyashita, *Rubber wear: experiment and theory* J. Chem. Phys. 162, 074704 (2025)
 - [2] J.F. Archard, *Contact and rubbing of flat surfaces*, J. Appl. Phys. **24**, 981 (1953).

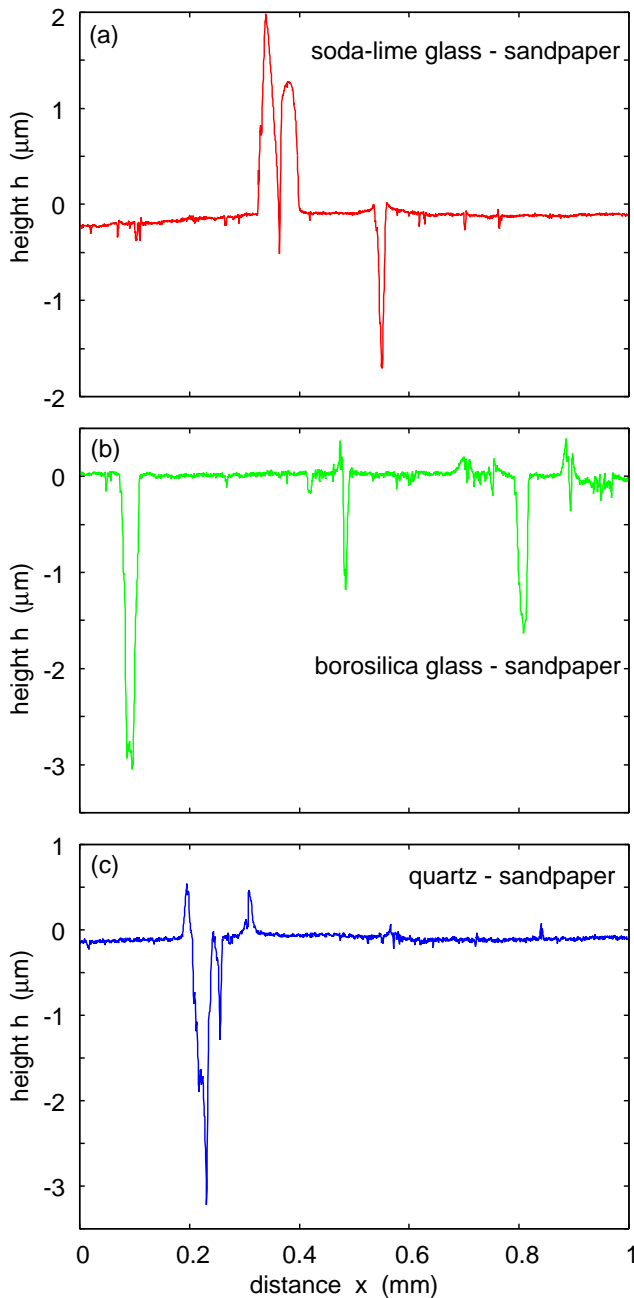


FIG. 20. The height profile orthogonal to the wear or ploughing tracks after a soda-lime glass block (a), boro-silica glass block (b), and a quartz block (c) was slid a short distance on a sandpaper P100 surface.

[3] R. Holm, *Electric Contacts*, Almqvist and Wiksell, Stockholm (1946)

[4] E. Rabinowicz, *The effect of size on the looseness of wear fragments*, *Wear* **2**, 4 (1958).

[5] E. Rabinowicz *Influence of surface energy on friction and wear phenomena*, *Journal of Applied Physics* **32**, 1440 (1961).

[6] R. Aghababaei, D.H. Warner and J.F. Molinari, *Critical length scale controls adhesive wear mechanisms*, *Nature Communications* **7**, 11816 (2016).

[7] L. Frerot, R. Aghababaei and J.F. Molinari, *A mechanistic understanding of the wear coefficient: From single to multiple asperities contact*, *Journal of the Mechanics and Physics of Solids* **114**, 172 (2018).

[8] J. Choudhry, A. Almqvist, R. Larsson, *Improving Archard's Wear Model: An Energy-Based Approach*, *Tribology Letters* **72**, 93 (2024).

[9] S. Pham-Ba and J.-F. Molinari, *Adhesive Wear Regimes on Rough Surfaces and Interaction of Micro-contacts*, *Tribology Letters* **69**, 107 (2021).

[10] R.S. Dwyer-Joyce, R.S. Sayles and E. Ioannides, *An investigation into the mechanisms of closed three-body abrasive wear*, *Wear* **175**, 133 (1994).

[11] T.C. Buttery and J.F. Archard, *Grinding and abrasive wear*, *PIOC. Inst. Mech. Eng.* **185** 537 (1971).

[12] Werner JH, Rosenberg JH, Keeley KL, Agrawal DK, *Immunobiology of periprosthetic inflammation and pain following ultra-high-molecular-weight-polyethylene wear debris in the lumbar spine* *Expert Rev Clin Immunol.* 2018;14(8):695-706. doi:10.1080/1744666X.2018.1511428

[13] R. Stoczek, *Some Revisions of Fatigue Crack Growth Characteristics of Rubber*, *Adv Polym Sci* https://doi.org/10.1007/12_2020_72

[14] A.N. Gent, *Adhesion and Strength of Viscoelastic Solids. Is There a Relationship between Adhesion and Bulk Properties?*, *Langmuir* **12**, 4492 (1996).

[15] P. Ghosh, R. Stoczek, M. Gehde, R. Mukhopadhyay and R. Krishnakumar, *Investigation of fatigue crack-growth characteristics of NR/BR blendbased tire tread compounds*, *Int. J. Fract.* **188**, 9 (2014).

[16] R. Rivlin and A. Thomas, *Rupture of rubber. I. Characteristic energy for tearing*, *J. Polymer Sci.* **10**, 291 (1953).

[17] J. Rong, J. Yang, Y. Huang, W. Luo and X. Hu, *Characteristic Tearing Energy and Fatigue Crack Propagation of Filled Natural Rubber*, *Polymers* **13**, 3891 (2021).

[18] M.H. Müser and A. Wang, *Contact-Patch-Size Distribution and Limits of Self-Affinity in Contacts between Randomly Rough Surfaces*, *Lubricants* **6** 85 (2018).

[19] B.N.J. Persson, *Theory of rubber friction and contact mechanics*, *The Journal of Chemical Physics* **115**, 3840 (2001).

[20] B.N.J. Persson, *Contact mechanics for randomly rough surfaces*, *Surface Science Reports* **61** 201 (2006).

[21] V. Lambert and E.E. Brodsky, *The competition between roughness and strength for scale-dependent surfaces*, *Phys. Rev. E* (in press).

[22] T.G. Bifano, T.A. Dow and R.O. Scattergood, *Ductile-mode grinding: A new technology for machining brittle materials*, *Journal of Engineering for Industry* **113**, 184 (1991).

[23] M.A. Davies, Y. Chou, and C.J. Evans, *On Chip Morphology, Tool Wear and Cutting Mechanics in Finish Hard Turning*, *CIRP Annals* **45**, 77 (1996).

[24] E.K. Antwi, K. Liu and H. Wang, *A review on ductile mode cutting of brittle materials*, *Front. Mech. Eng.* **13**, 251 (2018).

[25] U.D. Hangen, *Time-Dependent Deformation Behavior of PMMA*, Bruker Application Note # 1513 <https://industronnano.com/wp-content/uploads/2020/09/Polymer-AN1513-Rev-A0.Time-Dependent-Deformation-Behavior-of-PMMA-2018.pdf>

[26] W. Hong and Z. Xiulin, *The formulae of fatigue crack propagation in polymethyl methacrylate*, <https://www.gruppofrattura.it/ocs/index.php/ICF>

- /ICF10/paper/viewFile/5013/7020
- [27] E. Enriques, A. del Campo, J.J. Reinoso, G. Konstantopoulos, C. Charitidis, J.F. Fernandez, *Correlation between structure and mechanical properties in α -quartz single crystal by nanoindentation, AFM and confocal Raman microscopy* Journal of Materials Research and Technology **26**, 2655 (2023).
 - [28] M. Barlet, J-M Delaye, T. Charpentier, M. Gennisson, D. Bonamy, T. Rouxel, and C.L. Rountree, *Hardness and toughness of sodium borosilicate glasses via Vickers's indentation*, Journal of Non-Crystalline Solids **417-418**, 66 (2015).
 - [29] A. Dey, R. Chakraborty, and A.K. Mukhopadhyay, *Nanoindentation of Soda Lime-Silica Glass: Effect of Loading Rate*, International Journal of Applied Glass Science **2**, 144 (2011)
 - [30] J.A. Greenwood, *Metal Transfer and Wear* Frontiers in Mechanical Engineering **6**, 1 (2020).

